

Lattice Gluon and Ghost Propagators, and the Strong Coupling in Pure SU(3) Yang-Mills Theory: Finite Lattice Spacing and Volume Effects

Anthony G. Duarte,¹ Orlando Oliveira,¹ and Paulo J. Silva¹

¹*CFisUC, Department of Physics, University of Coimbra, P-3004 516 Coimbra, Portugal.*

The dependence of the Landau gauge two point gluon and ghost correlation functions on the lattice spacing and on the physical volume are investigated for pure SU(3) Yang-Mills theory in four dimensions using lattice simulations. We present data from very large lattices up to 128^4 and for two lattice spacings 0.10 fm and 0.06 fm corresponding to volumes of $\sim (13 \text{ fm})^4$ and $\sim (8 \text{ fm})^4$, respectively. Our results show that, for sufficiently large physical volumes, both propagators have a mild dependence on the lattice volume. On the other hand, the gluon and ghost propagators change with the lattice spacing a in the infrared region, with the gluon propagator having a stronger dependence on a compared to the ghost propagator. In what concerns the strong coupling constant $\alpha_s(p^2)$, as defined from gluon and ghost two point functions, the simulations show a sizeable dependence on the lattice spacing for the infrared region and for momenta up to $\sim 1 \text{ GeV}$.

I. INTRODUCTION

The computation of the gluon and ghost propagators of pure Yang-Mills theory in the Landau gauge have been investigated in the past years using lattice simulations for the SU(2) and SU(3) groups and accessing deeper the infrared region. In four dimensions, this effort established a consensus that the gluon propagator [1–9] is infrared suppressed and acquires a finite non-vanishing value at zero momentum. On the other hand, the ghost propagator seems to be described essentially by its tree level expression [2, 3, 5, 10–14]. In order to access the infrared momenta, the lattice simulations have been performed on huge volumes: $(27 \text{ fm})^4$ using a 128^4 lattice for the SU(2) gauge group [1] and $(17 \text{ fm})^4$ using a 96^4 lattice for SU(3). Such large volumes were achieved by setting the lattice spacing at $\sim 0.2 \text{ fm}$. Although the simulations were performed within the perturbative scaling window, the use of such large lattice spacings rise the question of how far from the continuum limit the results are.

For pure Yang-Mills theory the mass scale is given by the mass of the lightest glueball state. For SU(3), lattice simulations [15, 16] show that the lightest glueball has the quantum numbers $J^{PC} = 0^{++}$ and a mass of about 1700 MeV. The distance scale associated with such a value for the mass being $a \sim 0.12 \text{ fm}$. For the SU(2) gauge group [17], the predicted lightest glueball is about 1600 MeV and the corresponding distance scale is given again by 0.12 fm. It follows, that the large lattice spacings used in the simulation mentioned in the previous paragraph can introduce some bias on the final result. Indeed, in [8], the dependence of the gluon propagator on the lattice spacing for the SU(3) gauge group was analysed. The authors conclude that not only the effects due to the use of a large lattice spacing are dominant, over the finite volume effects, but also that the computations using such a large lattice spacing underestimates the propagator in the infrared region. However, at the qualitative level the results of [8] reproduce the large volume/large lattice spacing simulations reported in [1, 3].

In the current paper, we aim to extend the work of [8]

and investigate the dependence of the gluon and ghost propagators on the lattice spacing for large physical volumes $\gtrsim 6.5 \text{ fm}$. Furthermore, given that from the gluon and ghost propagator one can define a renormalisation group invariant strong coupling constant $\alpha_s(p^2)$, we also analyse the dependence of the coupling on the lattice spacing. Our results show that the use of a large lattice spacing changes the deep infrared values of the gluon propagator, of the ghost propagator and of the strong coupling constant. The simulations reported here show that the gluon propagator is suppressed in the infrared region, when one uses a large lattice spacing, while the ghost propagator is enhanced by using a larger lattice spacing. On the other hand, for the definition of the strong coupling constant considered here, the use of a larger lattice spacing enhances α_s for low and mid momenta up to $p \lesssim 1 \text{ GeV}$.

The paper is organised as follows. In Sec. II we resume the details of the lattice calculations, including definitions, number of configurations, Landau gauge fixing and the renormalization procedure. In Sec. III A we report on the computation of the gluon propagator, while in Sec. III B we report on the results for the ghost propagator. In Sec. III C the results for the running coupling are discussed. In Sec. IV we compare our simulations with the lattice results of [3]. Finally, in Sec. V we summarise the results discussed and conclude.

II. LATTICE SETUP AND RENORMALIZATION PROCEDURE

The pure gauge SU(3) Yang-Mills simulations reported here use the Wilson action at several β values and physical volumes. The full set of simulations performed in the context of this work is resumed in Tab. I. For the conversion into physical units we use the string tension as measured in [18].

The gauge configurations were generated with the Chroma library [20] using a combined Monte Carlo sweep of seven overrelaxation updates with four heat bath

β	a (fm)	$1/a$ (GeV)	L	La (fm)	Conf	Sources
5.7	0.1838(11)	1.0734(63)	44	8.087	100	3
6.0	0.1016(25)	1.943(47)	64	6.502	100	2
			80	8.128	70	2
			128	13.005	35	1
6.3	0.0627(24)	3.149(46)	128	8.026	54	3

TABLE I: Lattice setup. The physical scale was set from the string tension as measured by [18]. The lattice spacing for $\beta = 6.3$ was not measured in [18], so we relied on the procedure described in [19]. The last column refers to the number of point sources, per configuration, used in the inversion of the Faddeev-Popov matrix needed to compute the ghost propagator.

updates. Each configuration $U_\mu(x)$ obtained from the Monte Carlo sampling was gauge fixed to the Landau gauge by maximising the functional

$$F_U[g] = \frac{1}{V N_d N_c} \sum_{x,\mu} \text{Re Tr} [g(x) U_\mu(x) g^\dagger(x + \hat{e}_\mu)] \quad (1)$$

over the gauge orbit and where V is the number of the lattice points, $N_d = 4$ the number of space-time dimensions, $N_c = 3$ the number of colours and \hat{e}_μ the unit vector along the direction μ . In what concerns the gauge fixing algorithm, we rely on the Fourier accelerated steepest descent method [21], which was implemented using Chroma and PFFT [22] libraries. The quality of the gauge fixing was monitored by

$$\theta = \frac{1}{V N_c} \sum_x \text{Tr} [\Delta(x) \Delta^\dagger(x)] , \quad (2)$$

where

$$\Delta(x) = \sum_\nu [U_\nu(x - \hat{e}_\mu) - U_\nu(x) - h.c. - \text{trace}] , \quad (3)$$

which is the lattice version of the gauge fixing condition $\partial A = 0$. For each gauge configuration, the gauge fixing was stopped when $\theta \leq 10^{-15}$.

The Landau gauge gluon propagator is given by

$$D_{\mu\nu}^{ab}(p) = \delta^{ab} \left(\delta_{\mu\nu} - \frac{p_\mu p_\nu}{p^2} \right) D(p^2) , \quad (4)$$

where latin indexes refer to colour degrees of freedom and greek indexes to Lorentz degrees of freedom, and its computation was done using the set of definitions described in Ref. [23]. The results reported here are given as function of the tree level improved momentum

$$p_\mu = \frac{2}{a} \sin \left(\frac{n\pi}{L_\mu} \right) , \quad n = 0, 1, \dots, \frac{L_\mu}{2} \quad (5)$$

where a is the lattice spacing and L_μ the number of lattice points in the direction μ . The statistical errors on the

propagators were evaluated using the bootstrap method with a confidence level of 67.5%.

The ghost propagator is defined as

$$G^{ab}(p) = \delta^{ab} G(p^2) \quad (6)$$

and we have relied on the method described in [24] to compute the scalar function $G(p^2)$. For most of the ensembles, we have considered several sources and their results averaged, in order to reduce the statistical noise. The statistical errors for the ghost propagator were computed as for the gluon propagator.

In the current paper, besides the propagators we also look at the renormalization group invariant strong coupling defined by

$$\alpha_s(p^2) = \frac{g_0^2}{4\pi} d_D(p^2) d_G^2(p^2) , \quad (7)$$

where

$$d_D(p^2) = p^2 D(p^2) \quad \text{and} \quad d_G(p^2) = p^2 G(p^2) \quad (8)$$

are the gluon and ghost dressing functions, respectively.

In order to compare the data of the various simulations, the propagators were renormalized using a MOM scheme with the renormalized propagators defined as

$$D(p^2)|_{p^2=\mu^2} = Z_A D_{Lat}(\mu^2) = \frac{1}{\mu^2} \quad (9)$$

and

$$G(p^2)|_{p^2=\mu^2} = Z_\eta G_{Lat}(\mu^2) = \frac{1}{\mu^2} \quad (10)$$

where D_{Lat} and G_{Lat} refer to the bare lattice propagators. In the current work we use $\mu = 4$ GeV for the renormalization scale. The renormalization constants Z_A and Z_η were computed by fitting the bare lattice propagators to the functional form

$$D(p^2) = z \frac{p^2 + m_1^2}{p^4 + m_2^2 p^2 + m_3^4} \quad (11)$$

in the range $p \in [0, 6]$ for the gluon propagator and

$$G(p^2) = z \frac{\left[\log \frac{p^2}{\Lambda^2} \right]^{\gamma_{gh}}}{p^2} \quad (12)$$

in the range $p \in [2, 6]$ for the ghost propagator. Then, we use the fits to impose the normalization conditions (9) and (10). We have checked that the fits reproduced the lattice data for momentum ~ 4 GeV. Furthermore, in all cases the $\chi^2/d.o.f.$ associated to the fits are below unit.

In order to reduce the lattice artefacts, for momenta above 1 GeV we have performed the conic cut as defined in [25]. For momenta below 1 GeV, the figures include all lattice data points.

Besides the finite size effects due to the simulation on a finite box, with a finite lattice spacing, any lattice calculation is imbued with Gribov noise. In the current work we do not attempt to estimate the effects coming from the choice of the various maxima of the functional (1). As discussed in e.g. [23, 26, 27], peaking different maxima of $F_U[g]$ can lead to small changes in the propagators in the infrared region.

III. PROPAGATORS AND STRONG COUPLING: HOW THEY CHANGE WITH THE LATTICE SPACING AND THE VOLUME

In this section we present the results of the simulations resumed in Tab. I, focusing on the dependence on the lattice spacing and physical lattice volume.

A. The Gluon Propagator

The data for the renormalised gluon propagator can be seen in figure 1. In the left plot, the lattice data for essentially the same volume ($V \sim 8$ fm) and different lattice spacings (0.18 fm, 0.10 fm and 0.063 fm) is compared, whereas the right plot outlooks the simulations performed with the same lattice spacing ($a \sim 0.10$ fm) but different physical volumes ($La = 6.5$ fm, 8.1 fm and 13.0). If the data of our simulations shows essentially no dependence on the physical volume for volumes above $(6.5 \text{ fm})^4$, it also reveals a non-trivial dependence of the propagator on the lattice spacing.

From Fig. 1 one concludes that for the same physical volume, using a larger lattice spacing has an impact on the gluon propagator for momenta up to $\lesssim 1$ GeV, with the larger lattice spacing underestimating the lattice data in the infrared region.

The relative importance of finite lattice spacing/finite volume effects confirms the results reported in [8].

B. The Ghost Dressing Function

For the ghost two point function we report on the dressing function $d_G(p^2)$ as defined in Eq. (8). The ghost dressing function for the simulations with a physical volume of about $(8 \text{ fm})^4$ (left plot) and the same lattice spacings but different physical volumes (right plot) can be seen in Fig. 2.

In what concerns the dependence on the lattice spacing, the figure shows that decreasing the lattice spacing, while keeping the same physical volume, suppresses the ghost propagator in the infrared region. The figure also shows that the data computed with our coarser lattice, i.e. the simulation performed with $\beta = 5.7$, differs from all the other simulations for momenta as large as 2 GeV. Indeed, for momenta up to 2 GeV, the $\beta = 5.7$ data is above the data of remaining simulations and, in this

sense, the coarser lattice provides an upper bound to the corresponding continuum correlation function. Recall that the behaviour of the gluon propagator is the opposite, i.e. the $\beta = 5.7$ gives a lower bound to the continuum gluon propagator. The results of the simulations with the smaller lattice spacings are compatible within one standard deviation only for momenta above ~ 1 GeV and in the infrared region the propagator is suppressed if the lattice spacing is decreased. Note, however, that within two standard deviations the dressing functions are compatible for almost the full range of momenta.

From the right panel of Fig. 2 one can conclude that, as for the gluon propagator, the dependence of the lattice data on the physical volume is very mild if any. Indeed, the three lattice simulations are compatible within one standard deviation for all momenta. The data for our largest physical volume has a larger statistical error, and seems not to be as smooth as the others, but this is possibly due to the limited statistical ensemble used in the calculation of the correlation function.

For completeness, in Fig. 3 we report on the ghost dressing function for all the simulations referred in Tab. I. The data for all the simulations agree within two standard deviations, with the exception of the $\beta = 5.7$ for a lattice using 44^4 points which overestimates the propagator.

C. The Running Coupling

The combination of dressing functions

$$\alpha_s(p^2) = \frac{g_0^2}{4\pi} d_D(p^2) d_G^2(p^2) \quad (13)$$

is a renormalization group invariant and defines a running coupling. As for the propagators, we also aim to understand how $\alpha_s(p^2)$ changes with the lattice spacing and volume. In the computation of the strong coupling constant, we have used the bare lattice functions.

The dependence of the strong coupling on the lattice spacing and physical volume is resumed in Fig. 4. In order to better illustrate the dependence on the physical volume and lattice spacing, for the strong coupling constant, the plots only include the data surviving the momentum cuts mentioned before. As can be observed from the right plot, the simulations show essentially no dependence on the physical volume. On the other hand, the left plot of Fig. 4 shows that, at low and mid momenta, i.e. for $p \lesssim 1$ GeV, the strong coupling constant $\alpha_s(p^2)$ is slightly suppressed for smaller lattice spacings. For momenta above ~ 1 GeV, the results of all the simulations become compatible.

Another feature of $\alpha_s(p^2)$ concerns the position of its maximum. Indeed, as can be seen in Fig. 4, the position of the maximum of the strong coupling constant, as a function of p^2 , seems to be independent of both the lattice spacing and physical volume and occurs for $p^2 \sim 250 \text{ MeV}^2$. However, in what concerns the numerical value of

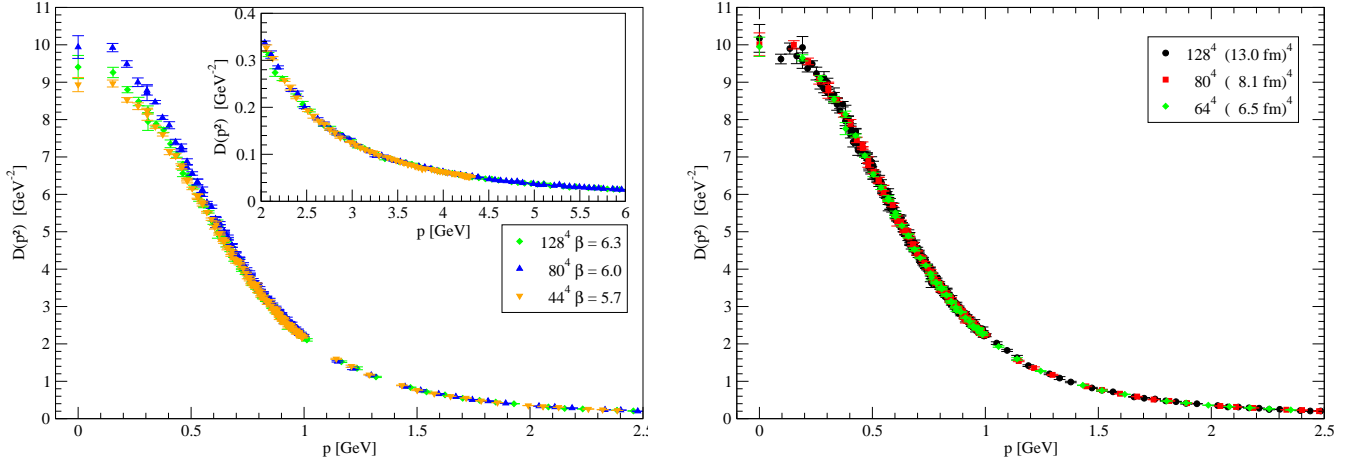


FIG. 1: Renormalised gluon propagator at $\mu = 4$ GeV for: (*left*) a physical volume of $(8 \text{ fm})^4$ and different lattice spacings; (*right*) the same lattice spacing and different volumes. Details about the lattice parameters are given in Tab. I.

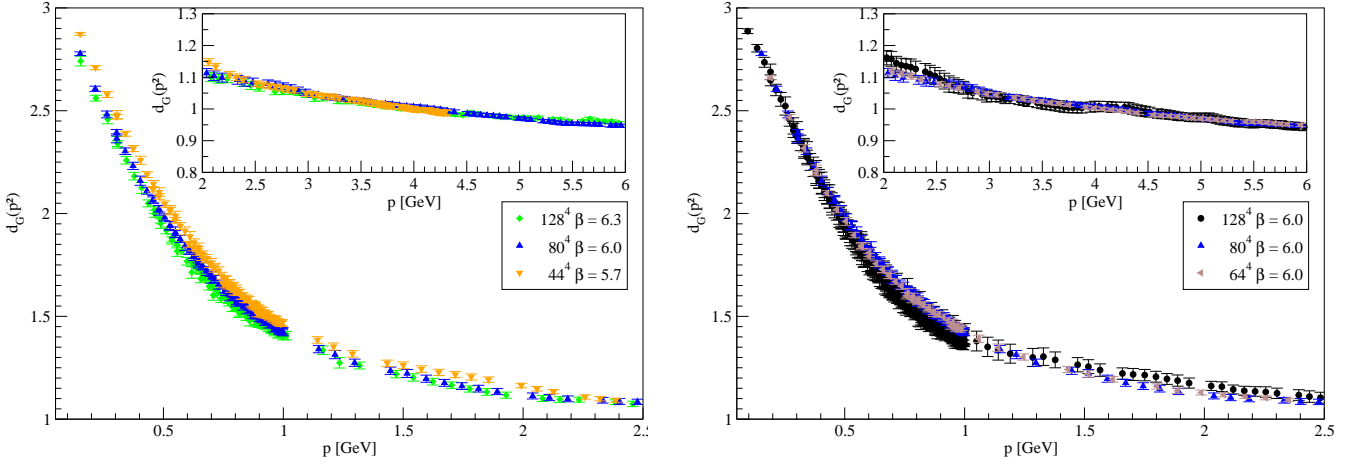


FIG. 2: Renormalised ghost dressing function at $\mu = 4$ GeV for: (*left*) a physical volume of $(8 \text{ fm})^4$ and different lattice spacings; (*right*) for the same lattice spacing and different volumes. Details about the lattice parameters are given in Tab. I.

the maximum of $\alpha_s(p^2)$, its value seems to be suppressed when approaching the continuum limit, i.e. for smaller lattice spacings. Indeed, our simulation at $\beta = 6.3$ shows a maximum of $\alpha_s(p^2)$ which is about 15% smaller compared to the corresponding value obtained for the remaining simulations.

IV. COMPARISON WITH PREVIOUS WORKS

In this section we aim to compare our lattice results with those performed using the, so far, largest physical volumes for an SU(3) simulation [3]. We call the reader's attention that in this work, the conversion into physical units relied on a different definition of the lattice spacing. In order to be able to compare these results with those reported in the previous sections, we have rescaled the

propagators accordingly. Another issue that should be taken into consideration is that our simulations and those of [3] used completely different algorithms to maximise the functional (1). As discussed previously, the choice of the maxima of $F_U[g]$ has an impact on the propagators, changing their behaviour in the infrared region (Gribov noise) and, therefore, the comparison of the results at low momenta should be done with care.

In Table II we summarise the lattice setup of the Berlin-Moscow-Adelaide simulations when one relies on our definition for the conversion into physical units.

A. The Gluon Propagator

In Fig. 5 we gather the results of our simulation at $\beta = 5.7$ with those of the Berlin-Moscow-Adelaide group.

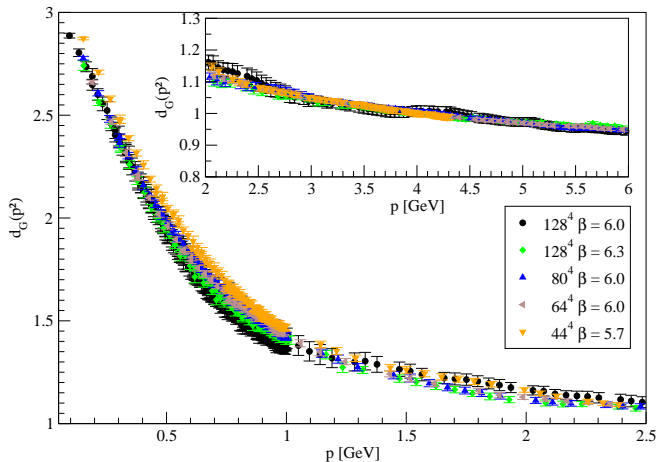


FIG. 3: Renormalised ghost dressing function at $\mu = 4$ GeV for the simulations reported in Tab. I.

β	a (fm)	$1/a$ (GeV)	L	La (fm)	# Conf	
					Glue	Ghost
5.7	0.1838(11)	1.0734(63)	64	11.763	14	14
			72	13.234	20	—
			80	14.704	25	11
			88	16.174	68	—
			96	17.645	67	—

TABLE II: Lattice setup considered by the Berlin-Moscow-Adelaide group [3]. Note that the data has been rescaled to use the same definition for all simulations — see text for details.

The data shows that the dependence on the volume is at most mild, with the infrared propagator decreasing slightly when La changes from 8 fm to 17 fm. Note that the differences occur only for momenta below ~ 400 MeV.

In Fig. 6 the two point gluon correlation function data reported previously, i.e. using larger (smaller) values of β (the lattice spacing) but smaller physical volumes, is compared with the largest volume result of the Berlin-Moscow-Adelaide group. All data sets seems to converge into a unique curve for momenta above ~ 0.7 GeV. For smaller momenta, the lattice data coming from the simulations at $\beta = 5.7$, which have the largest lattice spacing, are always below the remaining results. The comparison of the simulations performed at the smallest β values suggests that the propagators associated with the higher β should be multiplied by $\sim 8/9$, in the infrared region, to obtain the infinite volume limit.

B. The Ghost Dressing Function

The Berlin-Moscow-Adelaide ghost data covers momenta up to ~ 3 GeV ($\beta = 5.7, 64^4$) or up to ~ 1.5 GeV for the larger volume ($\beta = 5.7, 80^4$). Given that we are considering as renormalization scale $\mu = 4$ GeV,

one can not rescale the Berlin-Moscow-Adelaide data to compare with our simulations, as was done for the gluon propagator.

In Fig. 7 our data for the ghost dressing function obtained for $\beta = 5.7$ is compared with the results of the Berlin-Moscow-Adelaide collaboration. The bare lattice data from the 44^4 lattice simulation was rescaled to reproduce the 64^4 data at the highest available momentum. It follows that for momenta above ~ 700 MeV, the results of the various simulations define a unique curve. On the other hand, for smaller momenta the dressing function decreases as the physical volume of the lattice increases. This type of behaviour with the volume is not observed in our simulations where we used smaller lattice spacings. Indeed, as resumed in Fig. 2, our data shows essentially no dependence on the physical volume in the infrared region.

C. The Running Coupling

The comparison of the results for the strong coupling with those obtained by the Berlin-Moscow-Adelaide group can be seen in Fig. 8. The differences between the two sets of simulations are clearly seen for $p \lesssim 1$ GeV, with the estimations of [3] being smaller than those obtained in our simulations. In fact, some dependence on the lattice volume can be seen by comparing the different $\beta = 5.7$ data at low momenta. The results of all the simulations become compatible for momenta above ~ 1 GeV, as already described in Sec. III C.

V. SUMMARY AND CONCLUSIONS

In this work we report the dependence of the lattice results for the gluon propagator, the ghost propagator and the strong coupling constant on the physical volume and lattice spacing used to simulate QCD. Our goal is to understand how precise one can compute these functions using lattice QCD simulations, modulo possible effects associated with the presence of Gribov copies. In fact, the issue of the Gribov copies can be important to the calculation of the propagators and, possibly, the strong coupling constant [23, 26–28]. However, due to the huge amount of computer time needed to study Gribov copies effects in these large lattices, we are unable to disentangle such influence in our lattice results. Nevertheless, the observed dependence of the above mentioned functions on the lattice spacing and physical volume is, as demonstrated by the results discussed here and [8], far from trivial and impact mainly in the low momentum region.

In what concerns the gluon propagator the new simulations reproduce the behaviour already observed in [8]. The lattice data show essentially no dependence on the lattice physical volume for volumes above $(6.5 \text{ fm})^4$ for the full range of momenta accessed. On the other hand, the infrared propagator reveals a non trivial de-

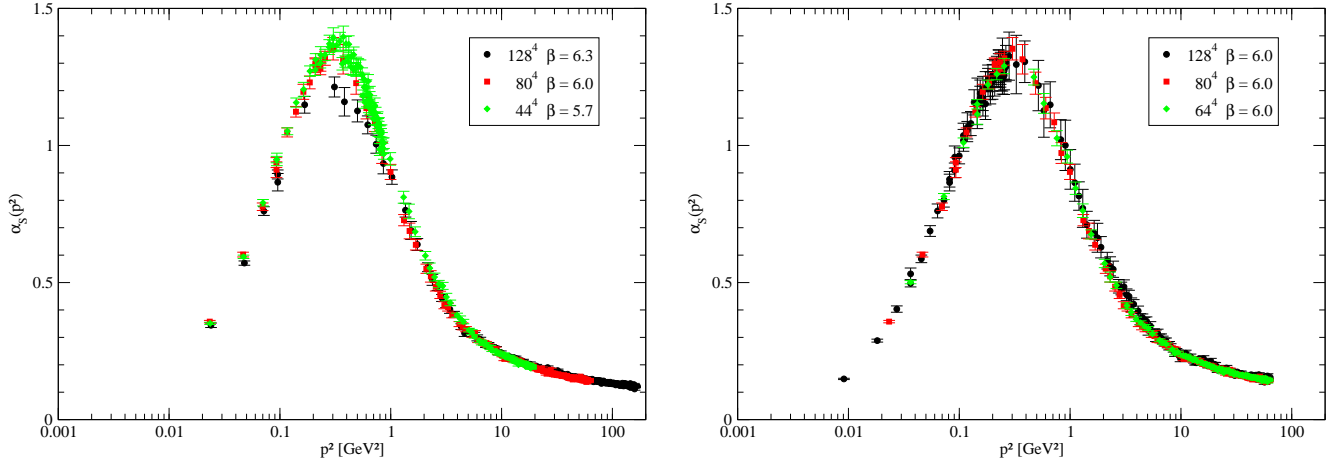


FIG. 4: Running coupling at $\mu = 4$ GeV for a physical volume of $(8 \text{ fm})^4$ and different lattice spacings (*left*) and for the same lattice spacing and different volumes (*right*). Details about the lattice parameters are given in Tab. I.

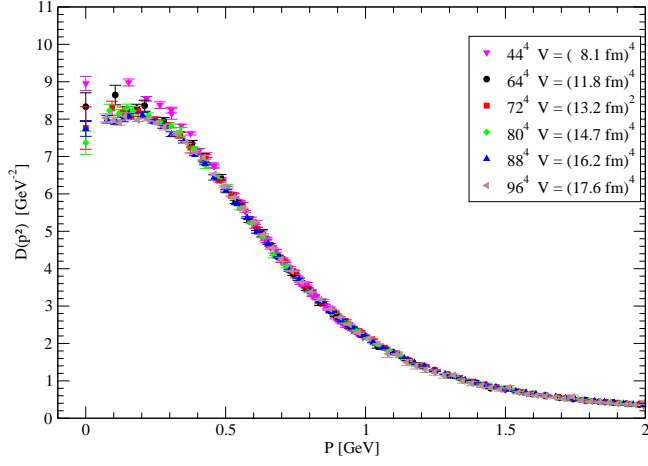


FIG. 5: Renormalized gluon propagator for the Berlin-Moscow-Adelaide lattice data. The plot also includes the results of our simulation with the same β value.

pendence on the lattice spacing, with smaller lattice spacings favouring larger infrared propagators for momenta smaller than ~ 1 GeV.

On the other hand, the ghost propagator has a mild dependence on the lattice volume but, contrary to the gluon propagator, the simulations show that this two point correlation function is suppressed at low momenta when the lattice spacing is decreased. We would like to point out that, for the ghost propagator, the functional form (12) which reproduces the perturbative one-loop result at high momentum is able to describe the lattice data over a surprisingly wide range of momenta. Indeed, if one takes Λ as fitting parameter, (12) is able to fit the lattice data from momenta ~ 1 GeV up to the largest momenta simulated. If one sets $\Lambda \sim \Lambda_{QCD} \sim 200$ MeV, the range of momenta described by (12) starts from about ~ 2 GeV

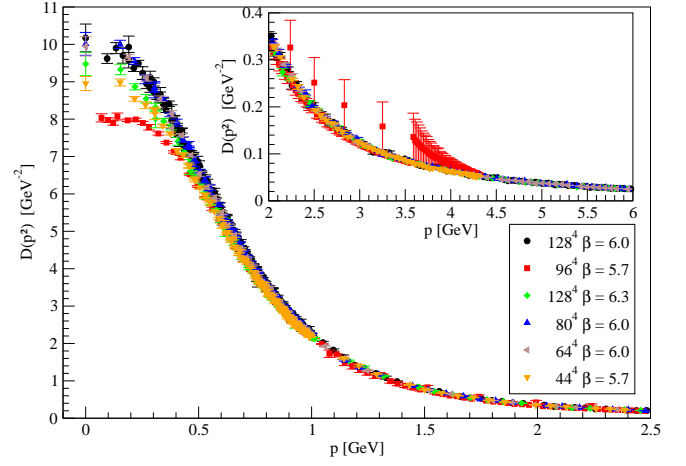


FIG. 6: All data sets including the largest volume of the Berlin-Moscow-Adelaide group. The inset shows a close-up of the high-momentum region, where all data sets define a unique curve.

and goes, again, up to the largest momentum available. We take this result as an indication that the ghost propagator follows closely the perturbative propagator for momenta as small as ~ 1 GeV.

From Figs. 1 and 2 one can quantify how the propagators are modified by changing the lattice spacing. For the gluon propagator one finds, for zero momentum, a $\sim 10\%$ order of magnitude effect by decreasing the lattice spacing from 0.18 fm down to 0.06 fm. In what concerns the ghost propagator, the change of the lattice spacing changes the propagator by $\sim 7\%$ at the lower momenta available in our simulations.

The dependence of the strong coupling constant on the lattice spacing and physical volume is milder than for the propagators. Although the position of the maximum

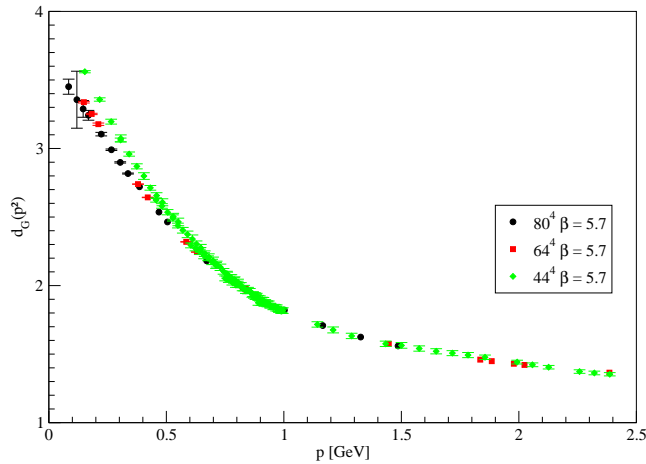


FIG. 7: Bare ghost dressing function from $\beta = 5.7$ simulations. The smallest lattice volume was rescaled to reproduce the 64^4 Berlin-Moscow-Adelaide numbers at its largest momentum.

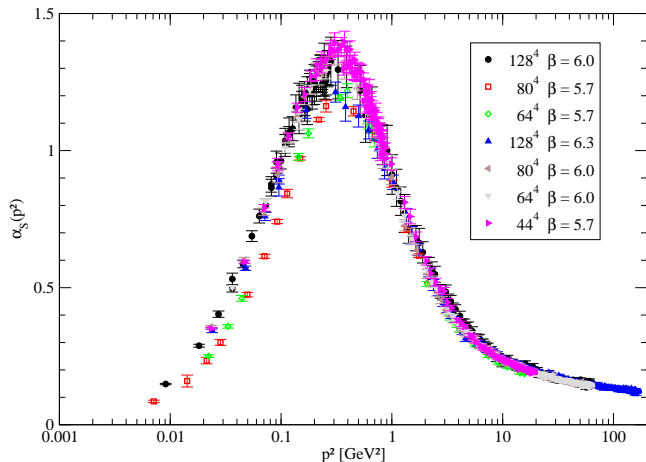


FIG. 8: Comparison of the results for the strong coupling computed from the simulations reported in Tab. I and Tab. II.

of $\alpha_s(p^2)$ seems to be independent of the both the lattice spacing and volume, the value of the strong coupling constant seems to be suppressed as one approaches the continuum limit. As discussed in Sec. III C, the value of $\alpha_s(p^2)$ at the maximum is reduced by $\sim 15\%$ for our largest value, when compared to the other calculations.

In Sec. IV our results are compared with those obtained using the largest physical volumes to simulate pure Yang-Mills SU(3) theory [3]. Such large volumes were achieved by relying on a large lattice spacing $a = 0.18$ fm. Our simulations and those performed by the Berlin-Moscow-Adelaide group give different answers for all the quantities considered here at low momenta. Note, how-

ever, that at the qualitative level the propagators and the strong coupling constant are similar. Furthermore, looking at the renormalized data, see Figs. 1 for the gluon and Fig. 5 for the ghost data, both sets of propagators show no dependence or a very mild one on the physical volume. The differences that are seen in the infrared for the two sets of simulations may be explained by different choices of the gauge fixing algorithm, i.e. in principle it can be attributed to Gribov noise. Indeed, it is well known that the choice of the maxima of $F_U[g]$ can change the propagators in the low momenta region. A direct comparison of the Berlin-Moscow-Adelaide simulations and ours for $a = 0.18$ fm, suggests that the continuum gluon (ghost) propagator should be suppressed (enhanced) at low momenta.

In summary, our results show that the computation of the two point correlation functions on the lattice has a non-trivial dependence on the lattice spacing and a mild dependence on the lattice volume for volumes above $(6.5 \text{ fm})^4$. Simulations performed with large lattice spacings, i.e. $a \gtrsim 0.18$ fm for pure Yang-Mills theory, are able to get the qualitative features of the propagators but introduce a measurable bias on the results at low momenta. The use of such large lattice spacings introduce also strong lattice spacing effects for all momenta range, not show here, which are removed for momenta above ~ 1 GeV by performing cuts on the momenta [25]. All the simulations discussed here use the Wilson action; certainly, improving the action may ameliorate the results in what concerns the dependence on the lattice spacing. However, relying on improved actions requires revising all the calculation procedure.

Acknowledgments

The authors acknowledge the Laboratory for Advanced Computing at University of Coimbra for providing HPC computing resources (Milipeia, Centaurus and Navigator) that have contributed to the research results reported within this paper (URL <http://www.lca.uc.pt>). The authors also acknowledge computing resources provided by the Partnership for Advanced Computing in Europe (PRACE) initiative under DECI-9 project COIMBRALATT and DECI-12 project COIMBRALATT2. P. J. Silva acknowledges support by F.C.T. under contract SFRH/BPD/40998/2007. The authors thank Balint Joo and Robert Edwards for helpful discussions concerning the use of Chroma, and Michael Pippig for the use of PFFT. This work was partially supported by projects CERN/FP/123612/2011, CERN/FP/123620/2011 and PTDC/FIS/100968/2008, projects developed under initiative QREN financed by UE/FEDER through Programme COMPETE.

-
- [1] A. Cucchieri, T. Mendes, PoS (**LAT2007**), 297 (2007) [arXiv: 0710.0412]
 - [2] A. Cucchieri, T. Mendes, O. Oliveira, P. J. Silva, Phys. Rev. D**76**, 114507 (2007) [arXiv:0705.3367]
 - [3] I. L. Bogolubsky, E.-M. Ilgenfritz, M. Müller-Preussker, A. Sternbeck, Phys. Lett. B**676**, 69 (2009) [arXiv:0901.0736]
 - [4] D. Dudal, O. Oliveira, N. Vandersickel, Phys. Rev. D**81**, 074505 (2010) [arXiv:1002.2374]
 - [5] E.-M. Ilgenfritz, C. Menz, M. Müller-Preussker, A. Schiller, A. Sternbeck, Phys. Rev. D**83**, 054506 (2011) [arXiv:1010.5120]
 - [6] O. Oliveira, P. Bicudo, J. Phys. G**38**, 045003 (2011)
 - [7] A. Cucchieri, D. Dudal, T. Mendes, N. Vandersickel, Phys. Rev. D**85**, 094513 (2012) [arXiv:1111.2327]
 - [8] O. Oliveira, P. J. Silva, Phys. Rev. D**86**, 114513 (2012) [arXiv:1207.3029]
 - [9] A. Sternbeck, M. Müller-Preussker, Phys. Lett. B**726**, 396 (2013)
 - [10] A. Sternbeck, E.-M. Ilgenfritz, M. Müller-Preussker, Phys. Rev. D**73**, 014502 (2006) [arXiv: hep-lat/0510109]
 - [11] O. Oliveira, P. J. Silva, Braz. J. Phys. **37**, 201 (2007) [arXiv: hep-lat/0609036]
 - [12] A. Cucchieri, T. Mendes, Phys. Rev. D**78**, 094503 (2008) [arXiv:0804.2371]
 - [13] A. Cucchieri, T. Mendes, Phys. Rev. D**88**, 114501 (2013) [arXiv:1308.1283]
 - [14] A. Cucchieri, D. Dudal, T. Mendes, N. Vandersickel, arXiv:1602.01646
 - [15] Y. Chen, A. Alexandru, S. J. Dong, T. Draper, I. Horváth, F. X. Lee, K. F. Liu, N. Mathur, C. Morningstar, M. Peardon, S. Tamhankar, B. L. Young, J. B. Zhang, Phys. Rev. D**73**, 014516 (2006) [arXiv: hep-lat/0510074]
 - [16] A. Chowdhury, A. Harindranath, J. Maiti, arXiv:1509.07959
 - [17] M. Teper, hep-th/9812187
 - [18] G. S. Bali and K. Schilling, Phys. Rev. D**47**, 661 (1993)
 - [19] P. J. Silva, O. Oliveira, P. Bicudo, N. Cardoso, Phys. Rev. D**89**, 074503 (2014) [arXiv:1310.5629]
 - [20] R. G. Edwards, B. Joo (SciDAC Collaboration, LHPC Collaboration, UKQCD Collaboration), Nucl. Phys. Proc. Suppl. **140**, 832 (2005) [arXiv: hep-lat/0409003]
 - [21] C. T. H. Davies, G. G. Batrouni, G. R. Katz, A. S. Kronfeld, G. P. Lepage, K. G. Wilson, P. Rossi, B. Svetitsky, Phys. Rev. D**37**, 1581 (1988)
 - [22] M. Pippig, SIAM J. Sci. Comput. **35**, C213 (2013)
 - [23] P. J. Silva, O. Oliveira, Nucl. Phys. B**690**, 177 (2004)
 - [24] H. Suman, K. Schilling, Phys. Lett. B**373**, 314 (1996)
 - [25] D. B. Leinweber, J. I. Skullerud, A. G. Williams, C. Parrinello, Phys. Rev. D**58**, 031501 (1998)
 - [26] P. J. Silva, O. Oliveira, PoS LAT2007 (2007) 333, arXiv:0710.0669 [hep-lat]
 - [27] A. Sternbeck, M. Müller-Preussker, Phys. Lett. B**726**, 396-403 (2013)
 - [28] A. Sternbeck, E.-M. Ilgenfritz, M. Müller-Preussker, A. Schiller, Phys. Rev. D**72**, 014507 (2005) [arXiv: hep-lat/0506007]